Supplemental File:

Case history

The decedent was a male born via vaginal delivery at 36.1 weeks of gestation to a 34-year-old woman, G3, P3, A1 (Gravida, para, abortus). He was conceived through in vitro fertilization with a sperm donor. He was born as a monochorionic, diamniotic twin. Ultrasound at the third trimester indicated the presence of slight microcephaly and smaller cerebellum which raised some concerns. He weighed 2.4 kg (0% Percentile, Z score -7.37), length of 43 cm (4^{th} Percentile, Z score -1.71) and head circumference of 30 cm (4^{th} percentile, Z score-1.79). The Apgar scores at 1 and 5 minutes after birth were recorded as 8 and 9. The decedent was discharged from the hospital 2 days after birth. At home he became apneic with hypoventilation and was readmitted to a hospital 4 days later. Despite positive airway pressure ventilation, the apneic spells continued which led to neurological and genetic investigations. He was then diagnosed with microcephaly and pontocerebellar hypoplasia with de novo CASK mutation. He displayed poor feeding, profound hypotonia, microcephaly, micrognathia, bilateral clubfoot, and vertical chordee with penile torsion. Oral-pharyngeal motility studies revealed mild to moderate oral motor dysphagia; there were episodes of silent aspirations with very limited reflux. A gastrostomy tube placement was performed. Fluctuations in body temperature with hypothermia and heart rate were also noted. Within 3 weeks after his birth, torso flexions were noted occurring 2-3 times a day. He also displayed tics in the hands, feet and neck which lasted for several seconds to several minutes. The decedent developed irritability and intolerance to feeds, hypothermia and acute respiratory failure with apnea. A surface, 25-channel video electroencephalography (vEEG) was performed using an international 10-20 system. A diagnosis of Ohtahara syndrome was established due to the presence of a typical burst suppression pattern. The heart rate varied between 90 and 150 beats per minute and displayed a sinus rhythm (Supplemental Figure 1). He was started on levetiracetam and a

ketogenic diet. The ketogenic diet seemed to impact the seizures adversely. Possibility of long-term palliative care including tracheostomy was discussed, but a decision was made against aggressive continued therapy. He passed away 2 months and 6 days after birth. The autopsy was conducted and the report prepared by an experienced pathologist (Julia Hegert) with aid from neuropathologists.

EEG Spectral Analysis

Raw data were trimmed for artifacts by a trained observer in the clinic. Data were analyzed in MATLAB 2017a using the EEGLab toolbox. After filtering from 0.01-50Hz, bad channels were removed based on spectral power. Spectral power was plotted for each channel independently using the spectopo() function with a window length of 256 samples, FFT length of 256, and 0 overlap in the entire 0.01-50Hz frequency band. Channels covering each of a given lobe (frontal, parietal, temporal, occipital, central) were then grouped and mean power spectral density was calculated within each biologically relevant frequency band: delta, alpha, beta, theta, and low gamma.

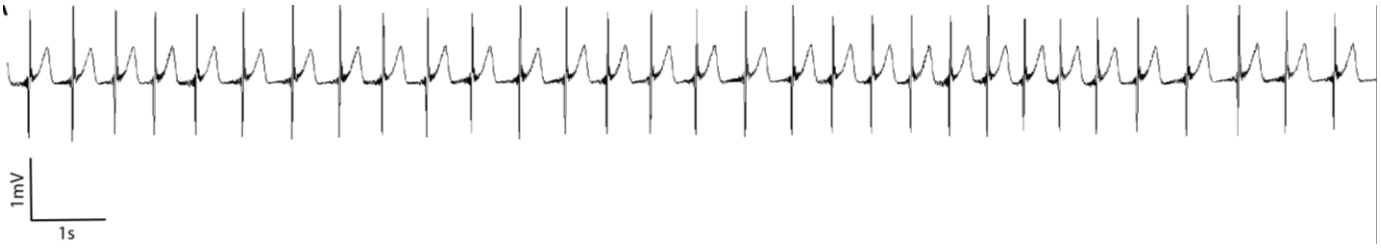

Supplemental Figure 1. (A) Representative 20 second electrocardiogram trace (precordial chest lead) demonstrating a sinus rhythm.

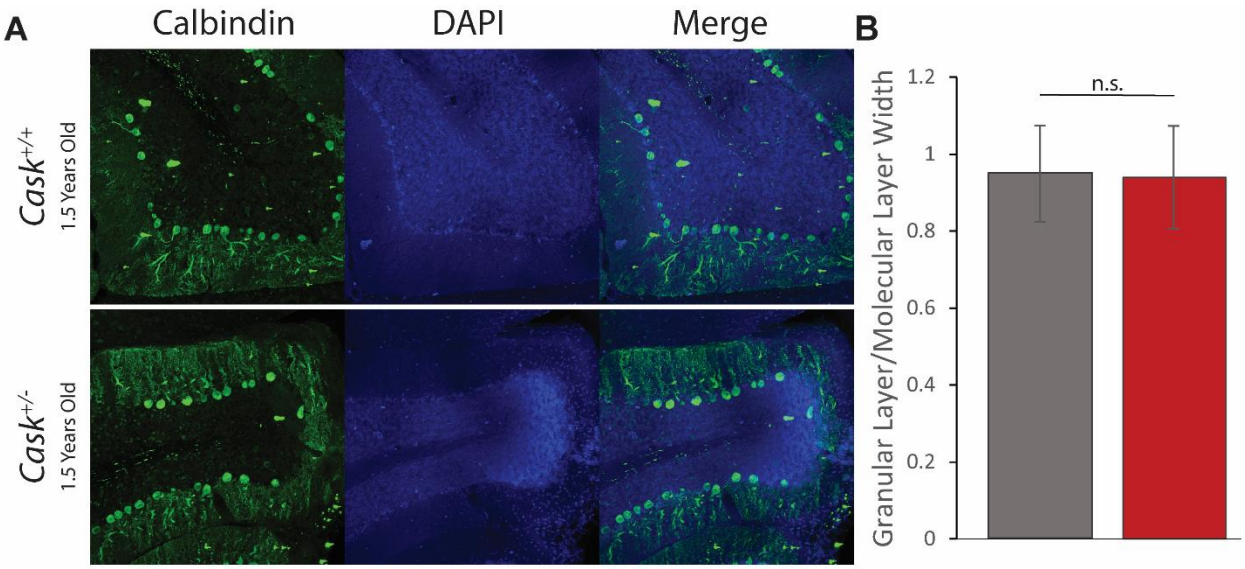

Supplemental Figure 2. (A) Representative images of cerebella from *Cask*$^{+/-}$ mice (bottom) and *Cask*$^{+/+}$ littermate control mice (top) aged up to 2 years. (B) Quantification of the ratio of the width of the granular layer over the molecular layer demonstrating no diminishment of granular layer width in the heterozygous absence of CASK even at extremely advanced ages. N=3 mice for each genotype.

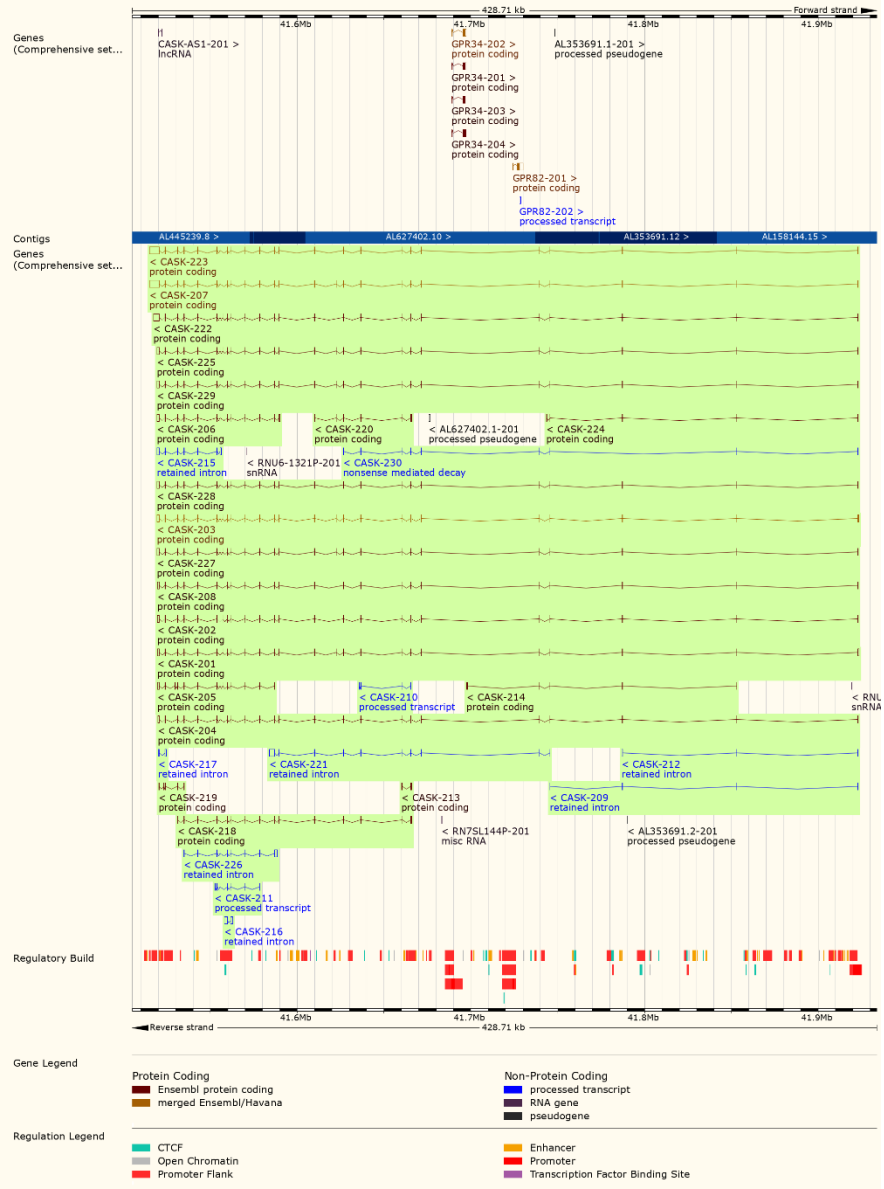

Supplemental Figure 3. NCBI summary of human *CASK* gene (top) and known splice variants (bottom). All functional transcripts include the second exon.

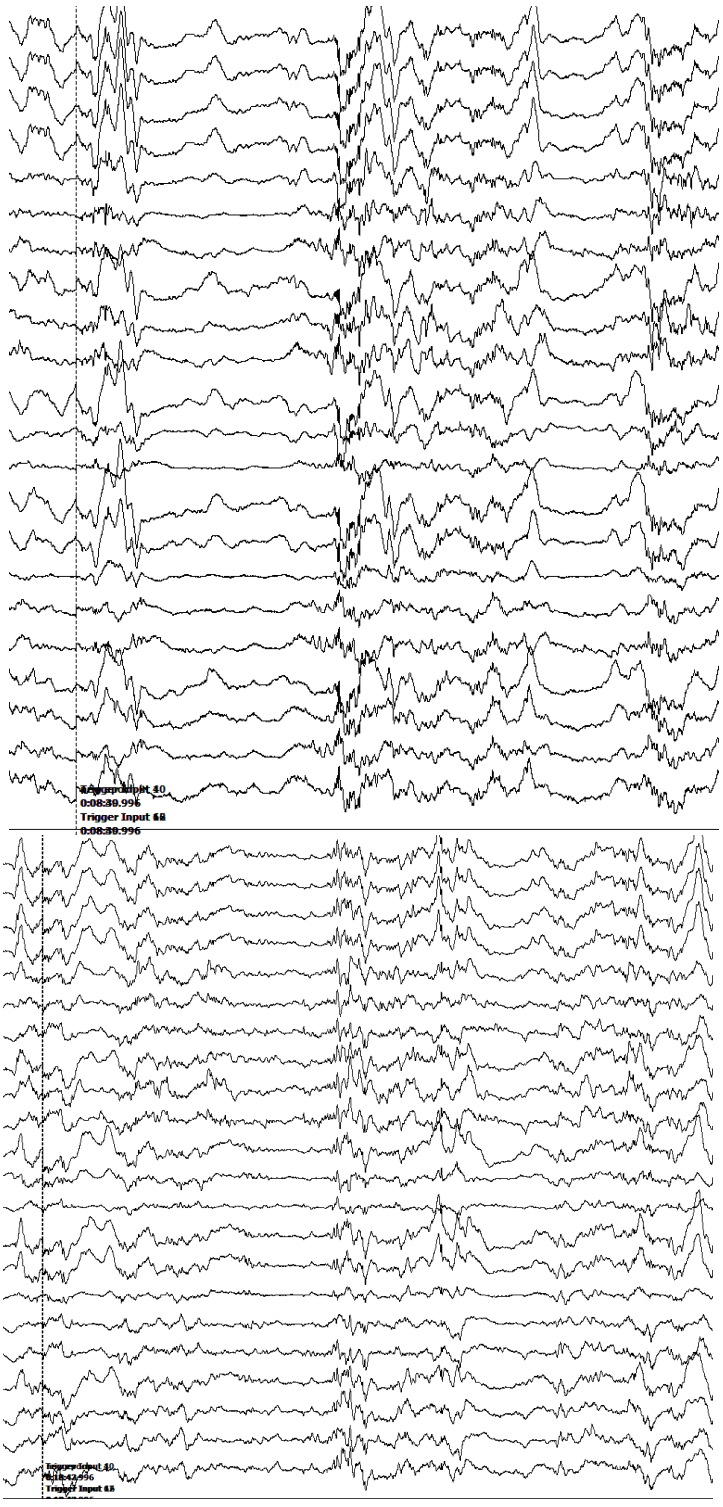

Supplemental Figure 4. Examples of burst-suppression pattern in EEG recordings.

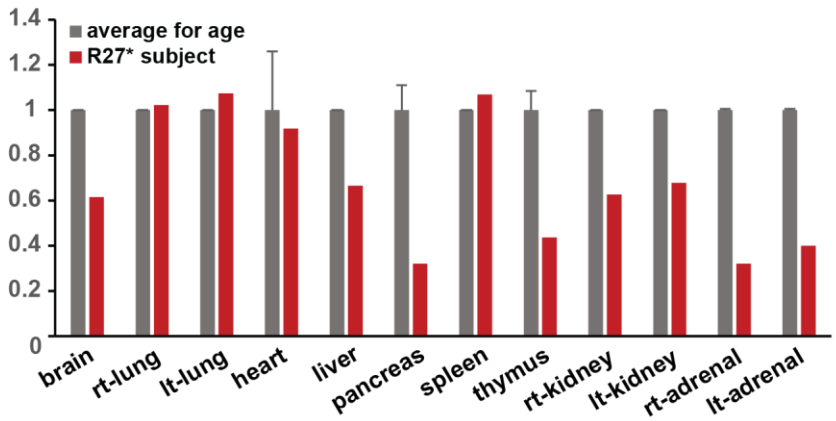

Supplemental Figure 5. Organ weights of the decedent compared to average respective organ weight for the age.

A

B

Supplemental Figure 6. Macroscopic view of 1 inch coronal slices of brain from (A) *CASK* R27Ter subject (2 months) (B) a child who died of non-neurological cause (40 days old). Note the disproportionate cerebellar and brain stem hypoplasia (white box). The grey and white matter configuration remains normal in *CASK* R27Ter subject. White matter tracts are unremarkable.

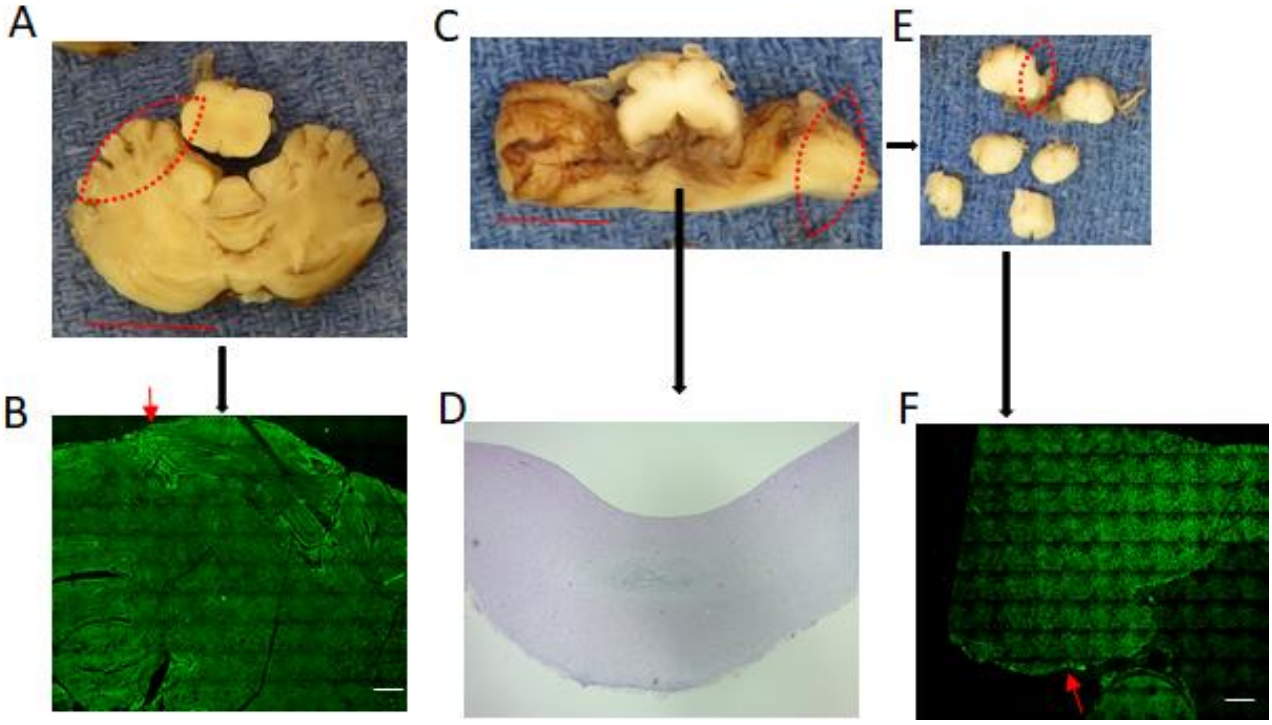

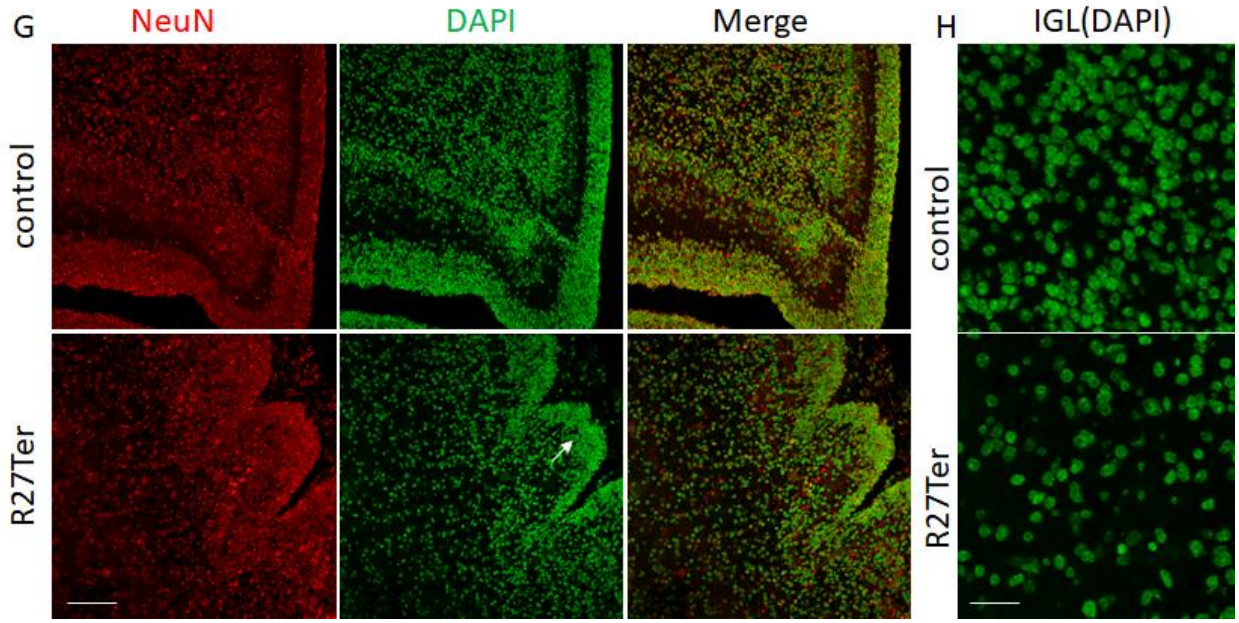

Supplemental Figure 7. A) Transverse section of cerebellum from the control case (white box supplemental Figure 6B). Scale bar =1cm. B) DAPI staining from a wide region of cerebellum from the indicated red circled region in A. Note the visibility of EGL and IGL at the edges (red arrow). Scale bar= 1mm. C) A similar transverse section from the boy with CASK R27* mutation showing nearly negligible thickness with a very rudimentary vermis. Scale bar= 1 cm. D) Hematoxylin-eosin staining of base of dilated 4th ventricle along with rudimentary vermis (2X). E) Sections from the lateral edge of the cerebellar hemisphere circled in red in C. F) DAPI staining

from a wide region of cerebellum from the indicated red circled region in E. Note thinning of EGL and yet no formation of IGL throughout the area (red arrow). Scale bar =1mm. G) Panels showing NeuN and DAPI labeling of control and R27Ter cerebellum as indicated, scale bar= 50μm. The white arrow indicates migrating granule cells in R27Ter. H) Magnified images of IGL from control and R27Ter cerebellum showing a highly depleted IGL in R27Ter cerebellum. Scale bar= 20μm.

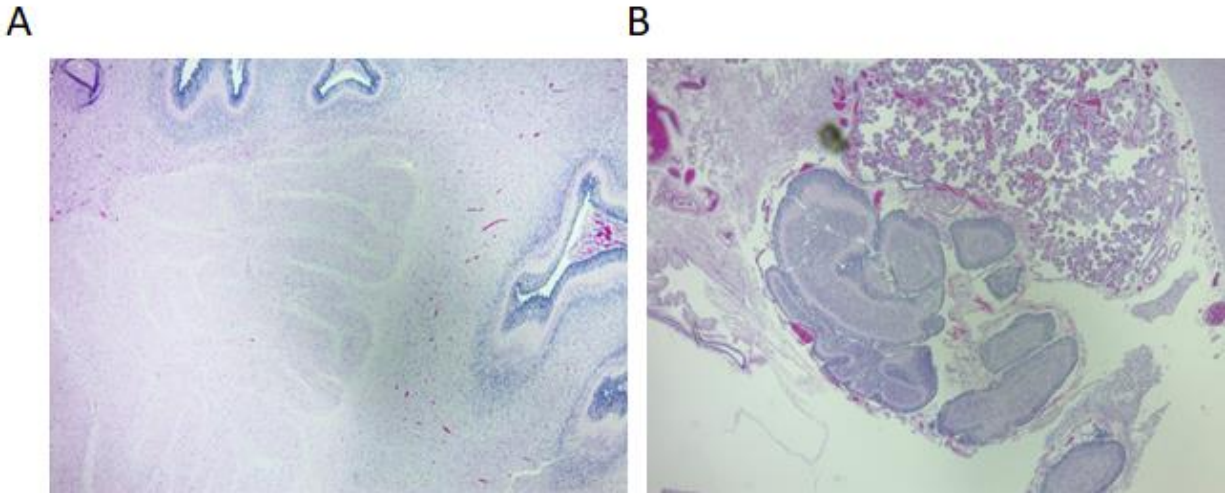

Supplemental Figure 8. A) Dentate nucleus shown from the control cerebellum, which is well formed (2X). B) Not much tissue remains at the region of the deep cerebellar nuclei in the boy with CASK R27* mutation. Complete absence of dentate nucleus is noted (2X).

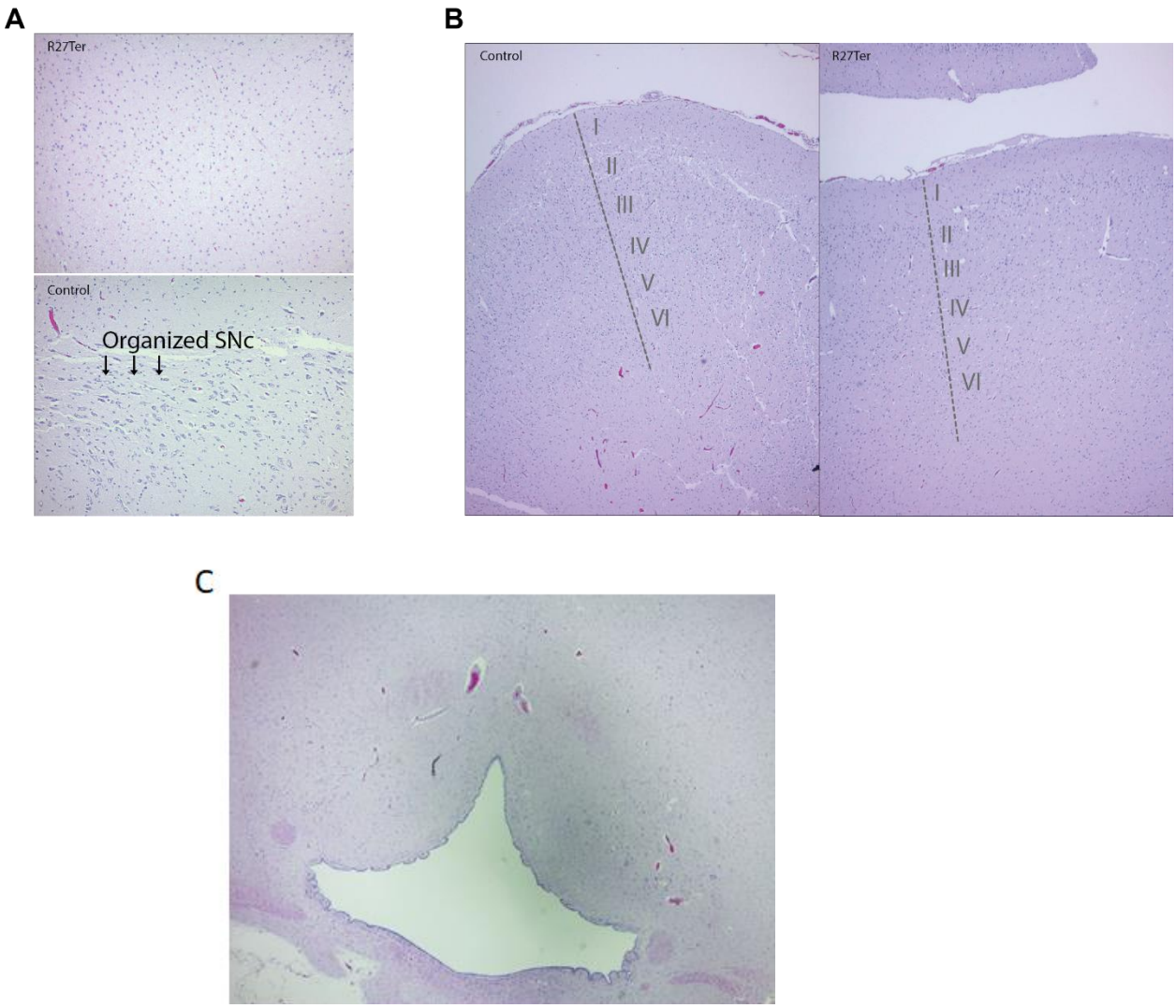

Supplemental Figure 9. Hematoxylin and eosin staining of the substantia nigra pars compacta (SNc) (A) and cerebral cortex (B) of the decedent and control. Note in (A) the absence of an organized SNc in the R27Ter subject which has cells with pink cytoplasm (astrocytes) but no neurons, large ordered blue-stained cells (neurons) are observed in the control. Note also the presence of a properly laminated cerebral cortex containing all six canonical layers. C) 2X section from the pons of the boy with R27* mutation. Note the presence of locus coeruleus.

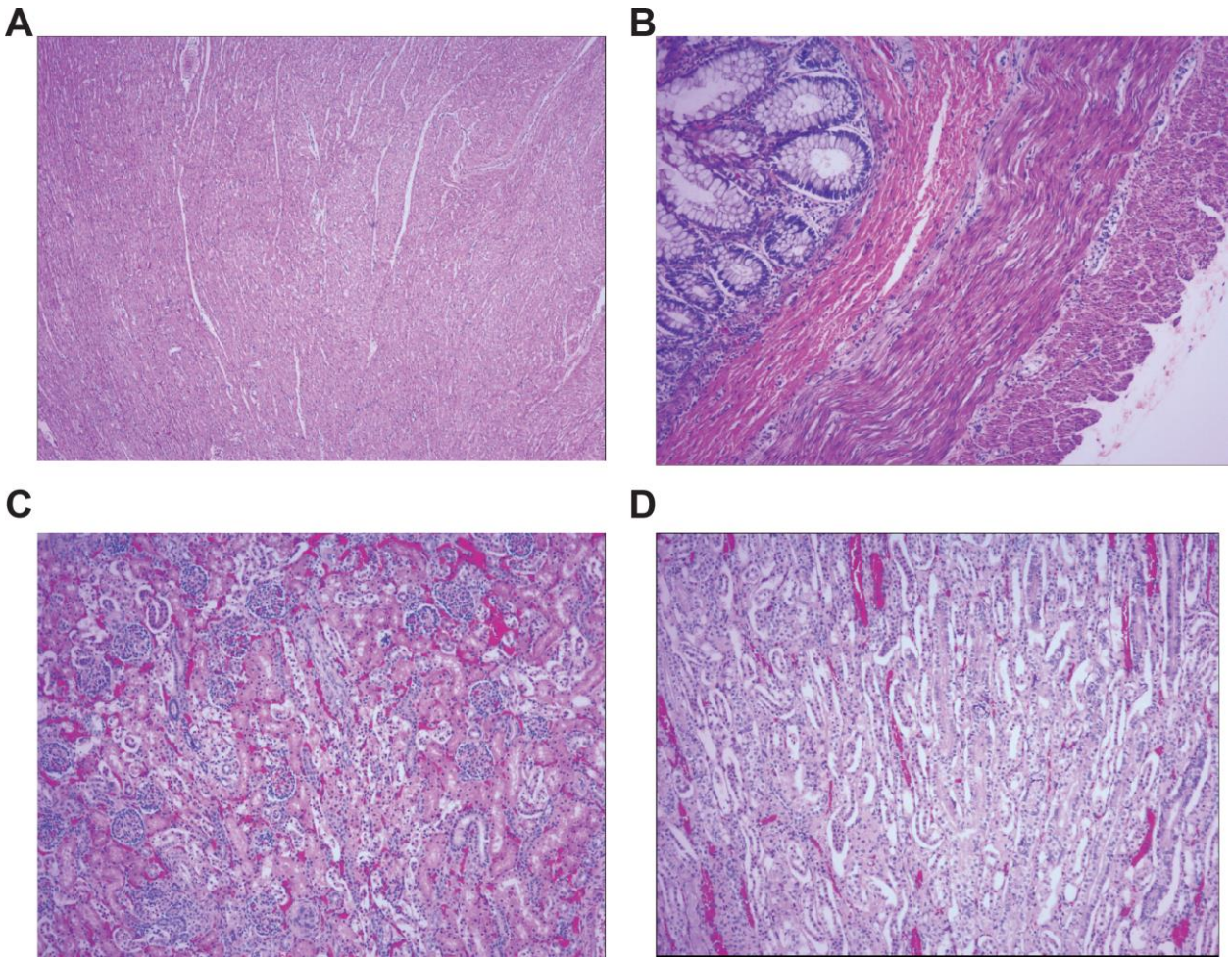

Supplemental Figure 10. Hematoxylin and eosin stain of (A) heart showing uniformly layered myofibers with no obvious pathology (4X), (B) rectum showing mucosal, submucosal, muscularis externa and serosal layers, neuronal plexuses are visible with no obvious pathology (10X), (C) renal cortex and (D) renal medulla showing normal glomeruli formation and renal tubules (10X).

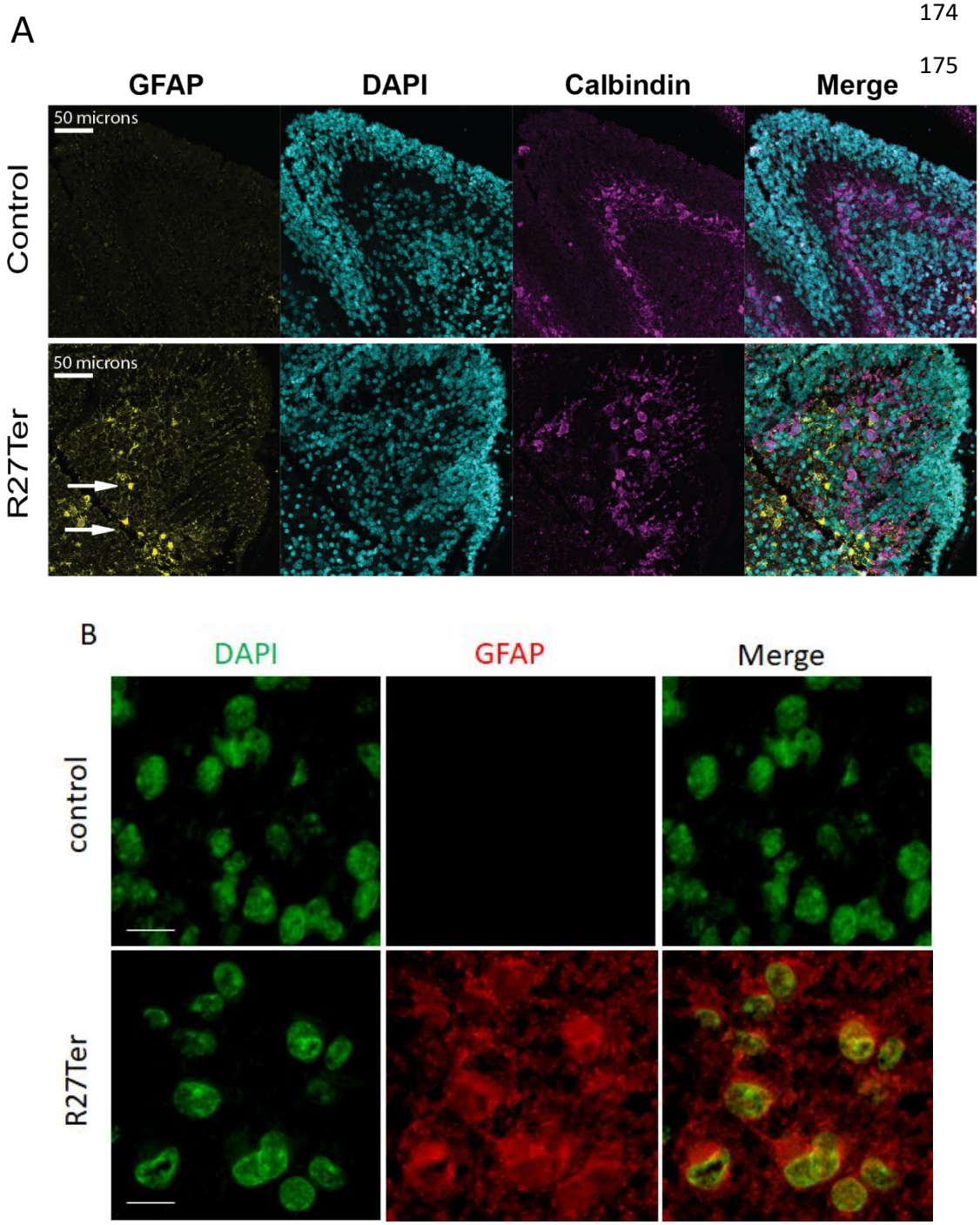

Supplemental Figure 11. A) Calbindin and GFAP immunostaining of the R27Ter (bottom) and control (top) subjects. Note the presence of properly aligned Purkinje cells in the R27Ter subject as indicated by calbindin immunoreactivity as well as the substantially increased GFAP immunoreactivity in the R27Ter subject relative to the control (astrocytic cells are indicated with white arrows). B) High magnification images of IGL from control and R27Ter cerebellum showing GFAP positive cells in R27Ter IGL. Scale bar = 10 μm.

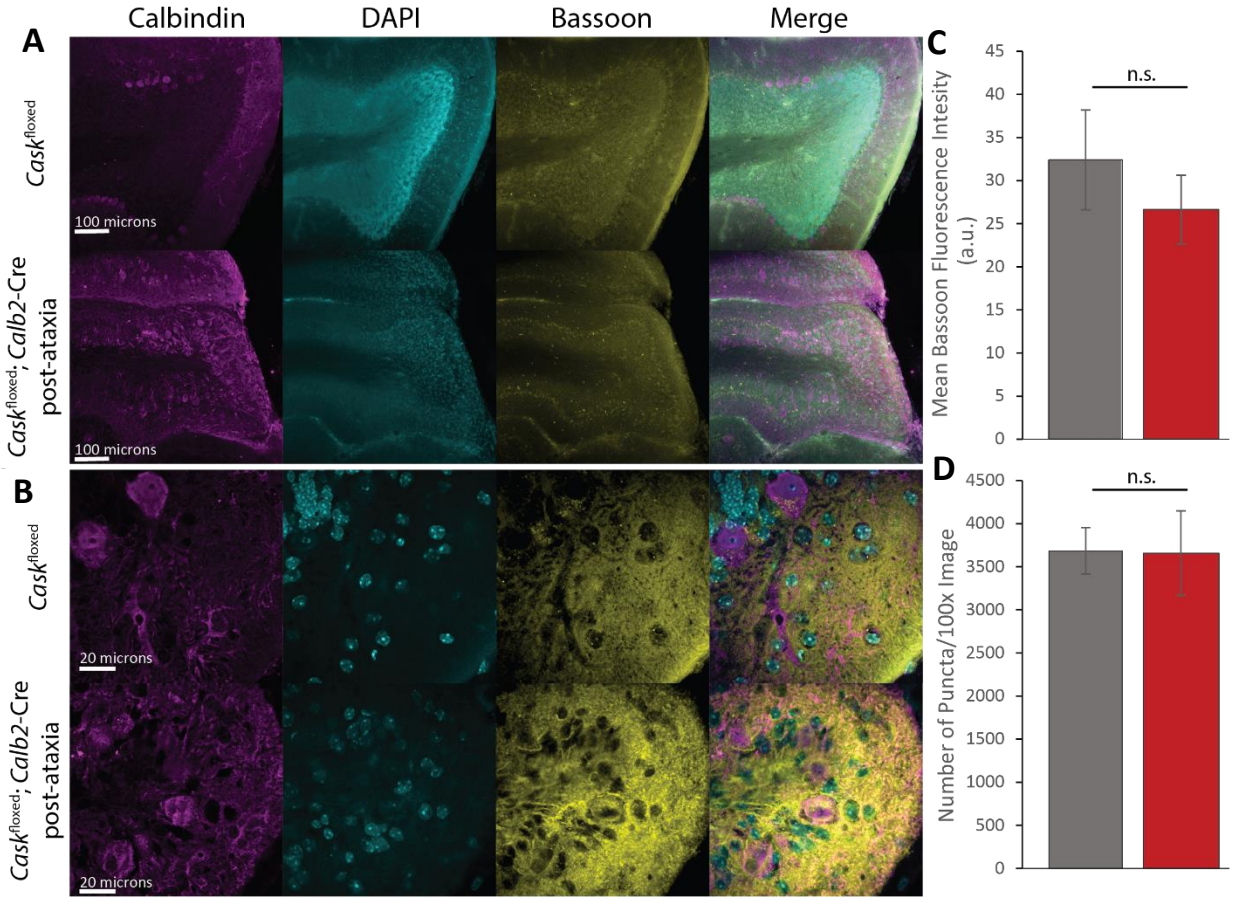

Supplemental Figure 12. (A) Representative 20x images of the anterior cerebellar folia in *Cask*^{floxed};*Calb2*-Cre post-ataxia plateau (bottom) and age-matched *Cask*^{floxed} controls (top) immunostained for calbindin to label Purkinje cells, DAPI to label nuclei, and bassoon to label synapses. (B) Quantification of bassoon staining intensity indicates no difference in fluorescence intensity between groups. (C) Representative 100x images of *Cask*^{floxed};*Calb2*-Cre post-ataxia plateau (bottom) and age-matched *Cask*^{floxed} controls (top). (D) Quantification of the number of bassoon positive puncta per 100x image quantified automatically using SynQuant (Wang et al. 2020) indicating no difference between groups. N=3 *Cask*^{floxed} and 4 *Cask*^{floxed};*Calb2*-Cre for (H-K); bars in all panels indicate mean±SEM. * indicates $p < 0.05$ using a two-tailed Student's t-test.

200

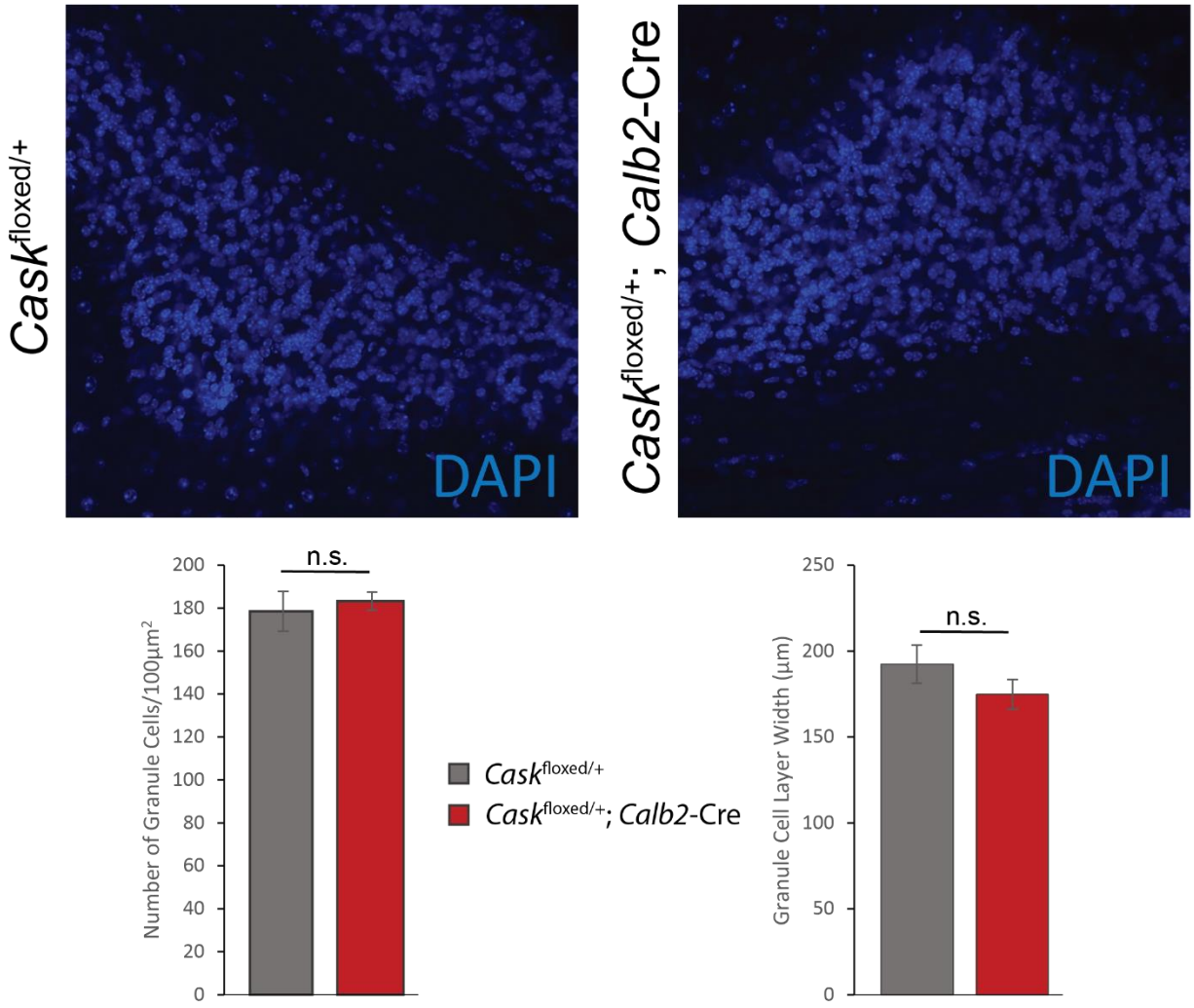

201 Supplemental Figure 13. Fluorescent images of nuclei in the granule cell layer for *Cask*$^{floxed/+}$
202 control mice (left) and *Cask*$^{floxed/+}$; *Calb2*-Cre heterozygous cerebellar knockout mice (right)
203 aged over 1 year. Quantification of DAPI+ nuclei density (left) and granular layer width (right)
204 demonstrating no degenerative cell death or thinning of the granular layer compared to control in
205 the heterozygous knockout; n=4 mice in each genotype.

206 Supplemental video

207 Video depicts a P100 *Cask*^{floxed};*Calb2*-Cre mice unable to take a single step without falling over.
208 The mouse is otherwise healthy and can survive with food and water on the cage floor. Note, the
209 righting reflex seems to be intact.